Front. Energy 2021, 15(3): 678–686
https://doi.org/10.1007/s11708-021-0768-6

RESEARCH ARTICLE

Zehong XU, Qiaohong ZHU, Xinguo XI, Mingyang XING, Jinlong ZHANG

Z-scheme CdS/WO_3 on a carbon cloth enabling effective hydrogen evolution

Abstract Photocatalytic water splitting for hydrogen (H_2) generation is a potential strategy to solve the problem of energy crisis and environmental deterioration. However, powder-like photocatalysts are difficult to recycle, and the agglomeration of particles would affect the photocatalytic activity. Herein, a direct Z-scheme CdS/WO_3 composite photocatalyst was fabricated based on carbon cloth through a two-step process. With the support of carbon cloth, photocatalysts tend to grow uniformly for further applications. The experimental results showed that the H_2 yield of adding one piece of CdS/WO_3 composite material was 17.28 μmol/h, which was 5.5 times as compared to that of pure CdS-loaded carbon cloth material. A cycle experiment was conducted to verify the stability of the as-prepared material and the result demonstrated that the H_2 generation performance of CdS/WO_3 decreased slightly after 3 cycles. This work provides new ideas for the development of recyclable photocatalysts and has a positive significance for practical applications.

Received Feb. 21, 2021; accepted May 31, 2021; online Sept. 10, 2021

Zehong XU, Qiaohong ZHU, Mingyang XING
Shanghai Engineering Research Center for Multi-media Environmental Catalysis and Resource Utilization, School of Chemistry and Molecular Engineering, East China University of Science and Technology, Shanghai 200237, China

Xinguo XI
School of Chemistry and Chemical Engineering, Yancheng Institute of Technology, Yancheng 224051, China

Jinlong ZHANG (✉)
Shanghai Engineering Research Center for Multi-media Environmental Catalysis and Resource Utilization, School of Chemistry and Molecular Engineering, East China University of Science and Technology, Shanghai 200237, China; School of Chemistry and Chemical Engineering, Yancheng Institute of Technology, Yancheng 224051, China
E-mail: jlzhang@ecust.edu.cn

Special Issue—Photocatalysis: From Solar Light to Hydrogen Energy (Guest Editors: Wenfeng SHANGGUAN, Akihiko KUDO, Zhi JIANG, Yuichi YAMAGUCHI)

Keywords photocatalysis, CdS/WO_3, carbon cloth, Z-scheme, hydrogen evolution

1 Introduction

Presently, the resources and environmental issues are becoming increasingly grave, and the search for clean alternatives to traditional fuels receives more and more attention [1,2]. Hydrogen, a fuel with the characteristics of non-toxicity, high calorific value, and harmless combustion product, has been considered as a potential option [3]. In 1972, Fujishima and Honda discovered for the first time that hydrogen could be obtained by photochemical decomposition of water by using titanium dioxide (TiO_2) [4]. Since then, the utilization of solar energy to produce hydrogen via water splitting with semiconductor photocatalyst has been regarded as a simple and effective method [5]. This method of storing solar energy in hydrogen in the form of chemical energy is viewed as one of the most promising ways to provide clean and renewable energy. Encouraged by this innovative discovery, photocatalytic hydrogen production has been studied extensively and the key to achieve better applications is to find photocatalysts with high reaction activities and enough stability.

To date, a variety of semiconductor photocatalysts have been prepared for hydrogen production and pollutant degradation, including metal oxides (TiO_2 [6], ZnO [7]), metal sulfides (CdS [8,9], ZnS [10], CuS [11]), carbon nitrides (g-C_3N_4 [12]) and so on [13]. CdS is a promising photocatalyst with a suitable band gap and an ideal conduction band edge [14]. However, owing to the strong recombination of photo-induced electron-hole pairs and the frequent occurrence of photocorrosion inside CdS, pure CdS is still far away from achieving large-scale industrial applications [15,16]. To solve the above problems, hybridization has been used as an efficient method to improve the separation of photoinduced electron-hole pairs. WO_3 is another promising photocatalyst for its

non-toxicity, high chemical stability, and moderate oxidizing ability [17]. Therefore, the rational design of WO_3 and CdS could be regarded as an effective strategy to improve the overall photocatalytic performance due to the fact that the formation of a Z-scheme system can be formed between them [18]. As reported [19–22], Z-scheme systems are designed to simulate photosynthesis in nature with the advantages of suppressing the recombination rate of photo-induced carriers by the combination of holes with a weak oxidizing ability and electrons with weak reducing abilities, thus accelerating charge transfer and separation. Hence, the reduction and oxidation catalytic centers are retained in two different regions, which obviously inhibited the occurrence of side reactions [18]. Many of the reported compound systems have chosen CdS as a component for hydrogen production, such as $CdS/BiVO_4$ [23], ZnO/CdS [24], CdS/Co_9S_8 [25], and $CdS/CdWO_4$ [26]. The effective utilization of sunlight is realized and the photocorrosion of CdS is inhibited.

Traditional photocatalysts are often investigated in powder form, which would cause difficulties in recycling and limit their industrial applications. Immobilization of photocatalysts is an effective method to deal with this dilemma. Carbon cloth (CT) is an ideal supporting material because of its characteristics of large specific surface area, uniform pore structure, and high surface adsorption reaction activity [27]. More importantly, the use of carbon cloth as support can ensure that materials with nanostructure features grow uniformly and produce hierarchical structures [28]. Recently, several photocatalytic systems have been constructed on the surface of carbon cloth successfully. Li et al. [28] reported a method that calcined in air after hydrothermal reaction, which successfully supported porous SnO_2 sheets on the surface of carbon cloth. The synthesized composites had a good stability and realized selective reduction of CO_2. Furthermore, compared with rigid carriers [29], the flexibility of carbon cloth makes it easy to use in different shape reactors and easier to recycle.

Herein, a two-step hydrothermal method was applied to prepare WO_3 and CdS onto the surface of carbon cloth, and the combination of the two photocatalysts was successfully achieved. A Z-scheme system composite photocatalyst without additional electron transmission medium was prepared, which effectively improved the separation efficiency of photogenerated carriers. Scanning electron microscopy (SEM) was used to visually observe the loading on the composite photocatalyst carbon cloth. X-ray electron diffraction (XRD) and X-ray photoelectron spectroscopy (XPS) analysis confirmed that WO_3 and CdS achieved a good combination on carbon cloth. The experimental results of photocatalytic hydrogen production showed that the hydrogen production rate of the WO_3/CdS composite prepared was 5.5 times as compared to the pure CdS-loaded carbon cloth material. Moreover, the stability of the prepared materials through cycling experiments was verified, and the results indicated that the photocatalytic hydrogen production activity did not decrease significantly after 3 cycles. At the same time, it was also found that the prepared composites had a good degradation activity, and degradation experiments of rhodamine B (RhB) were conducted. The design of an effective Z-scheme structure provides a new window for the preparation of efficient hydrogen evolution materials and has a positive impact on the practical applications of photocatalysts in the future.

2 Experimental

2.1 Chemical materials

All reagents were used without further purification. Hydrochloric acid (HCl, 36%–38%), Hexamethylenetetramine (HMT, > 98%), Sodium sulfide nonahydrate ($Na_2S \cdot 9H_2O$, AR), and Thioacetamide (TAA, > 99%) were supplied by Sinopharm Chemical Reagent Co. Ltd. (Shanghai, China). Anhydrous ethanol (EtOH, 99.5%), Sodium chloride (NaCl, > 99%), Sodium tungstate dihydrate ($NaWO_4 \cdot 2H_2O$, 99%), Cadmium chloride ($CdCl_2$, AR), and Anhydrous sodium sulfite (Na_2SO_3, > 98%) were purchased from Aladdin (Shanghai, China). Carbon cloth (CT, W0S1009) was purchased from Cetech Co. Ltd. (Taiwan, China). Deionized water with a conductivity of 18.25 MΩ·cm was used as solvent in all the experiments.

2.2 Sample preparation

Single-load WO_3 carbon cloth (W-CT): The synthesis steps of W-CT refer to the method reported by Huang et al. [30]. 1.056 g of $NaWO_4 \cdot 2H_2O$, 0.9 g of NaCl (as structure directing agent) [31], and 30 mL of H_2O were added into the inner tank of the hydrothermal kettle, and dissolved by magnetic stirring for 30 min. Then 3 mol/L of HCl was dripped into the mixed solution under continuous stirring to adjust the solution pH to 2. After stirring for 3 h, carbon cloth with a size of 1 cm × 1 cm was immersed into the solution, and the inner tank was put into the hydrothermal kettle. Then, the reaction kettle was placed in the oven of 180°C and reacted for 24 h. After the reaction, the reaction kettle was taken out and cooled to room temperature, and the carbon cloth was washed with ultra-pure water and EtOH respectively. After drying, the carbon cloth was placed in a muffle furnace and calcined at 450°C for 1 h, and the product W-CT was obtained.

Single-load CdS carbon cloth (Cd-CT): 20 mL of H_2O, 20 mL of EtOH, and 0.1464 g of $CdCl_2$ were added respectively into the tank of the hydrothermal kettle. After stirring uniformly, 0.448 g of HMT and 0.015 g of TAA were added to continue stirring for 30 min. Then, the carbon cloth was added to the solution, and the reaction kettle was placed in the oven at 180°C for 16 h. After the

reaction, the reaction kettle was taken out and cooled to room temperature, and the carbon cloth was washed with ultra-pure water and EtOH respectively. After drying, the product Cd-CT was obtained.

Dual-load WO_3 and CdS carbon cloth (WCd-CT): The as-prepared W-CT was immersed into a hydrothermal reactor containing the same mixed solution of $CdCl_2$, HMT, and TAA as above for hydrothermal growth, and CdS could be grown around WO_3. The product obtained was named WCd-CT.

2.3 Characterization

The loading of the catalyst on the carbon cloth surface was observed by scanning electron microscope. The crystal structure of the as-prepared samples was verified by an X-ray diffraction (Rigaku D/MAX 2550) with Cu Kα (40 kV, 100 mA). The chemical states around the surface elements were analyzed by an X-ray photoelectron spectroscopy (XPS, PHI 5000G ESGA). The UV-vis absorbance spectra were obtained for the dry-pressed disk samples using a Scan UV-vis spectrophotometer (Varian, Cary 500) equipped with an integrating sphere assembly, using $BaSO_4$ as the reflectance sample.

2.4 Photocatalytic hydrogen evolution

To assess the photocatalytic performance of the as-prepared materials, a photocatalytic H_2 evolution reaction was conducted in a top-irradiation Pyrex reaction vessel connected to a closed gas circulation and evacuation system. The system was vacuumized for 30 min to remove any residual air in the solution prior to light irradiation. For H_2 evolution, one piece of sample (or 30 mg of powder sample) was added in 100 mL of aqueous solution containing 0.1 mol/L of Na_2S and Na_2SO_3 as sacrificial reagent. After the system was degassed completely, the reaction solution was irradiated by a 300 W Xe lamp equipped with an AM 1.5 air mass filter. The evolved gases were analyzed by a gas chromatography equipped with a thermal conductive detector (TCD) and a 5 Å molecular sieve column, using Argon as the carrier gas.

2.5 Photocatalytic degradation

In a typical experiment, 50 mL of RhB aqueous solution (20 mg/L) was poured into a 50 mL photocatalytic tube, followed by the addition of the prepared sample (one piece). During the reaction, the solution was irradiated with a 300 W Xenon lamp equipped with an AM 1.5 air mass filter. Besides, the supernatant was withdrawn using a dropper at predetermined time intervals (every 10 min, 4 mL). The concentration of RhB was analyzed by using a UV-vis spectrophotometer (Varian, Cary 500).

3 Results and discussion

As illustrated in Fig. 1, the WCd-CT composite material was prepared through a two-step process. First, WO_3 particles were grown on CT by utilizing the hydrothermal method. SEM was used to observe the loading of WO_3 on the carbon cloth. As shown in Fig. 2(a), the surface of pure CT before the reaction was smooth and free of impurities. The growth of WO_3 particles on carbon fibers is demonstrated in Fig. 2(b), WO_3 powders grew well on the surface of the carbon cloth, and the catalyst on each rod-shaped fiber was fully loaded and uniformly distributed. The absence of excess powder in the gap between the fibers proved that the washing was adequate, and there was a strong interaction between the WO_3 powder and the fiber surface. Hence, the immobilization of catalyst was successful. The SEM image of Cd-CT is exhibited in Fig. 2(c). It can be observed that the powder adhesion

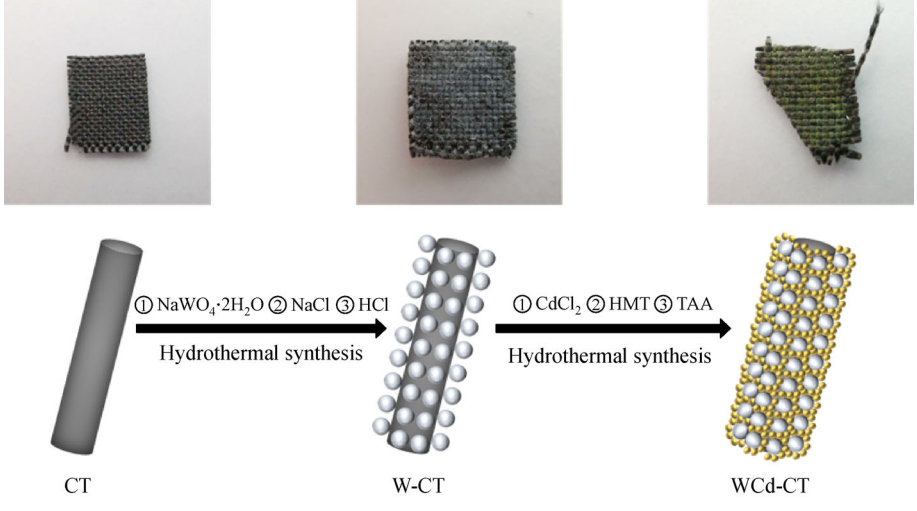

Fig. 1 Growth of WO_3 and CdS nanoparticles on CT.

amount was small in the entire range, manifesting that there was a weak interaction force between the CdS powder and the carbon fiber. Then, CdS was grown around WO_3 through the next hydrothermal reaction. The growth of CdS particles is displayed in Fig. 2(d). It can be clearly seen that the carbon fiber surface was covered with a thick layer of powder particles. Compared with the above-mentioned case where CdS loads alone on the fiber, it can indirectly explain the strong interaction between WO_3 and CdS. This good contact environment also provided advantages for the construction of suitable heterostructure between CdS and WO_3, and provided the possibility for the improvement of hydrogen production performance.

The XRD patterns of the prepared samples are depicted in Fig. 3. The characteristic diffraction peaks of CdS are marked by spheres, and the characteristic diffraction peaks of WO_3 are marked by triangles. The XRD pattern of CT shows a broad peak at around 25°, corresponding to the (002) plane of the graphite structure [32]. It is obviously observed that after the loading of WO_3, its characteristic diffraction peaks appear. The diffraction peaks at 13.957°, 22.718°, and 28.172° can be observed, which can be corresponded to (100), (001), and (200) crystal planes of hexagonal WO_3 (JCPDS card No. 33-1387), respectively. This indicates that WO_3 has been successfully loaded on the carbon cloth. Three characteristic peaks at 43.681°, 47.839°, 50.882° are observed in the XRD patterns, corresponding to (110), (103), (200) crystal planes of hexagonal CdS (JCPDS card No. 41-1049), respectively. As shown in Fig. 3(d), both the characteristic diffraction peaks of WO_3 and the characteristic peaks of CdS can be observed in the XRD patterns of the composite WCd-CT, confirming the existence of both CdS and WO_3. Combining the investigations above, CdS nanoparticles were successfully loaded around WO_3 on carbon cloth.

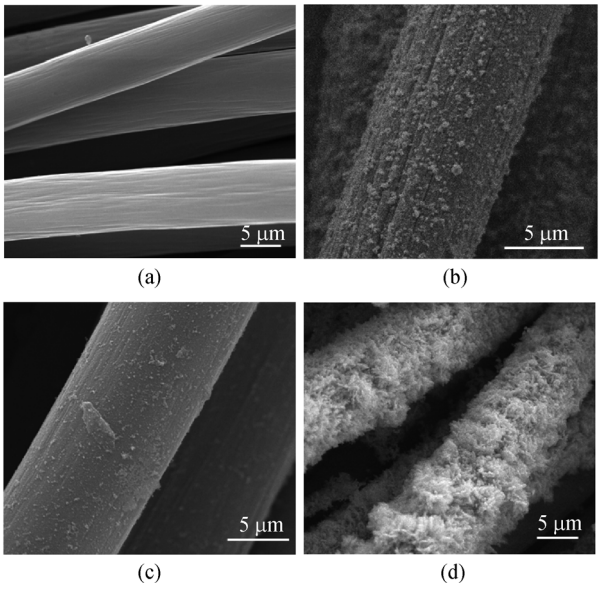

Fig. 2 SEM images of each sample.
(a) CT; (b) W-CT; (c) Cd-CT; (d) WCd-CT.

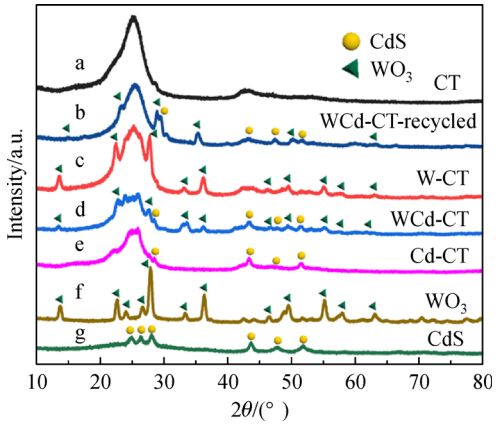

Fig. 3 X-ray diffraction patterns.

X-ray electron spectroscopy was used to detect the chemical states of W, O, Cd, and S on the surface of WCd-CT samples. The C 1s XPS peaks obtained from the test are displayed in Fig. 4(a), and the three peaks at 289.4, 286.2, and 284.5 eV imply that there are three different carbon chemical environments in the product. The two weak peaks at 286.2 eV and 289.4 eV can be assigned to C–O and C(O)OH, and the strong peak at 284.5 eV can be ascribed to the C–C band [33–35]. After loading different materials, the main peak of C remained basically unchanged, proving that the carbon cloth of the base material was very stable under various conditions. Figure 4(b) shows the analysis and comparison of the W element state on the single-load WO_3 carbon cloth, and the dual-load WO_3 and CdS carbon cloth. The peaks at 38.0 eV and 36.0 eV can be assigned to W $4f_{5/2}$ and W $4f_{7/2}$, respectively, indicating the presence of W^{6+} in the sample, and therefore verifying the fact that WO_3 is successfully loaded on the carbon cloth. After the loading of CdS, the peak of W shifted to a lower field, suggesting that the chemical state around W had changed. This also provides some evidence for the formation of the Z-scheme system between WO_3 and CdS, which is also consistent with some previous reports [36]. The Cd 3d XPS spectra are manifested in Fig. 4(c), in which the two peaks at 411.8 eV (Cd $3d_{3/2}$) and 405.0 eV (Cd $3d_{5/2}$) can be considered as Cd^{2+}. The Cd peaks of the double-loaded sample are basically the same as the peak position of the CdS-loaded sample, which further proves that CdS is well loaded on W-CT and the methods of directly growing CdS on carbon cloth and loading CdS after WO_3 growth are valid. As for S 2p XPS spectra (Fig. 4(d)), the peaks at 162.8 eV and 161.8 eV can be ascribed to S $2p_{1/2}$ and S $2p_{3/2}$, which further proves the existence of divalent S. This also demonstrates the successful synthesis of CdS. In addition, the high-resolution peak from WCd-CT shows a positive shift compared to those of Cd-CT, which shows that the electronic environment around S has changed,

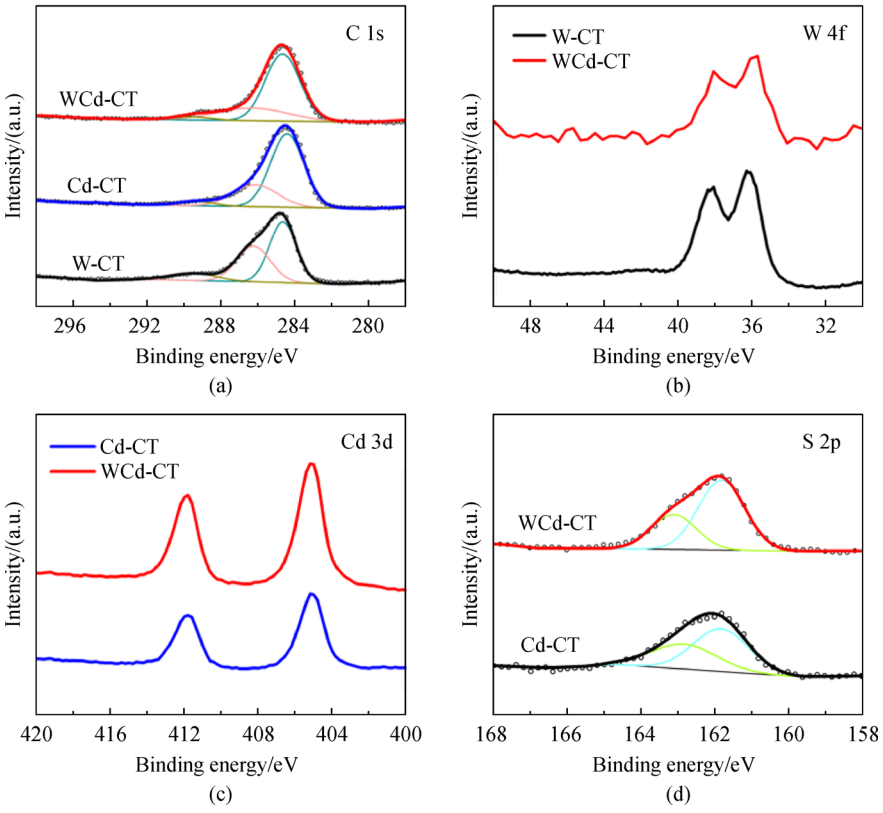

Fig. 4 XPS of W-CT, Cd-CT, and WCd-CT.
(a) C 1s; (b) W 4f; (c) Cd 3d; (d) S 2p.

further indicating that there is electron transfer between WO_3 and CdS. The successful loading of WO_3 and CdS on carbon cloth can be confirmed by the above results, and there is also an interaction effect between them.

The UV-vis diffuse spectra of CdS, WO_3, and CdS/WO_3 samples are presented in Fig. 5. The absorption edge of WO_3 is around 450 nm, attributing to its wide bandgap. After the loading of CdS, the CdS/WO_3 composite sample has a wider absorption in the visible light region, and its absorption edge is broadened to near 570 nm, which is very close to CdS. The photocatalytic hydrogen production activities of the as-prepared W-CT, Cd-CT, and WCd-CT were evaluated under the illumination of simulated sunlight, using $Na_2S \cdot 9H_2O$ and Na_2SO_3 as sacrificial reagents to quench photoinduced holes. The hydrogen yield of as-prepared samples is displayed in Figs. 6(a) and 6(b). For CT and W-CT, no obvious H_2 production was detected during the whole experiment. The reason for this is that the conduction band potential of a pure WO_3 material does not meet the thermodynamic requirements for H_2 evolution. Pure CdS exhibited a non-ideal H_2-evolution rate due to the rapid recombination of photo-induced charge carriers. Under the experimental condition of adding one piece of Cd-CT (loaded with 1.5 mg of CdS), only 7.88 μmol H_2 was produced within 150 min (3.15 μmol/h). In contrast, the photocatalytic hydrogen production rate of WCd-CT composite (loaded with 4.0 mg of WO_3/CdS) had been significantly improved, reaching 17.28 μmol/h (about 4.32 mmol/(g·h) under the same condition. It is believed that one main factor for improving the photocatalytic performance is the combination and intimate contact of WO_3 and CdS, which greatly promotes the separation of photo-induced electrons and holes, thus more electrons could migrate to the surface to participate in the photocatalytic water splitting to produce hydrogen. The reason for supporting photocatalyst on carbon cloth is to

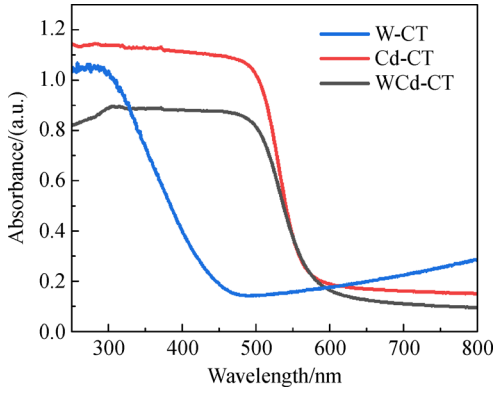

Fig. 5 UV-vis diffuse absorption spectra of CdS, WO_3, and CdS/WO_3 composites.

achieve better recovery and reuse. Therefore, the stability of the prepared photocatalyst needs to meet the requirement of multiple cycles. To this end, a photocatalytic hydrogen production cycle experiment was conducted. As shown in Fig. 6(c), the activity of the composite material does not decrease significantly after 3 cycles, indicating that the WCd-CT composite material has an excellent stability and could initially meet the requirements of recycling. In addition, the structure of WCd-CT after reaction was investigated. As shown in Fig. 3(b), the characteristic diffraction peaks of WO_3 and CdS can still be observed in the XRD patterns of recycled WCd-CT, indicating that WO_3 and CdS still exist on the carbon cloth. Moreover, it is also found that the carbon fiber surface of the recycled WCd-CT sample is still coated with a relatively complete catalyst layer, which is not significantly different from that before the reaction (Fig. S2, Electronic Supplementary Material).

To further understand the enhanced charge separation inside the prepared samples, the photocatalytic degradation activity of the prepared samples was evaluated by degrading RhB under simulated solar light irradiation. As shown in Fig. 6(d), the light source was not turned on during the period of −30–0 min, and a dark adsorption experiment was conducted for 30 min. The concentration of the solution was basically unchanged during this period, showing that the adsorption effect of the experimental system on RhB was negligible. Cd-CT displayed a poor photocatalytic activity, and only 8% of RhB was removed within 60 min. As for W-CT, 15% of RhB was removed under the same conditions, attributing to its relatively more positive VB (valence band) position. Moreover, the more loading of WO_3 on the same piece of carbon cloth than CdS which could be seen from SEM image might also be one of the reasons. Of the three as-prepared materials, WCd-CT had the best activity, which could be explained by the effective transfer and separation of photogenerated carriers.

To estimate the band gap of the semiconductors, the correlation curve of $(\alpha hv)^{n/2}$ and hv as well as its tangent line was drawn, where α, h, and v corresponded to the absorption index, Planck's constant and, the optical frequency, respectively. Moreover, the value of n depends on the type of semiconductor. For indirect band gap semiconductors, the value of n is 1, while for direct band gap semiconductors, the value of n is 4. According to Fig. 7, the band gaps of WO_3 and CdS were estimated to be about 2.65 eV and 2.25 eV, respectively, which is consistent with the previous reports [37]. The photocurrent transient diagrams of W-CT, Cd-CT, and WCd-CT samples are shown in Fig. 8(a). It can be seen that the photocurrent response is enhanced after the combination of CdS over

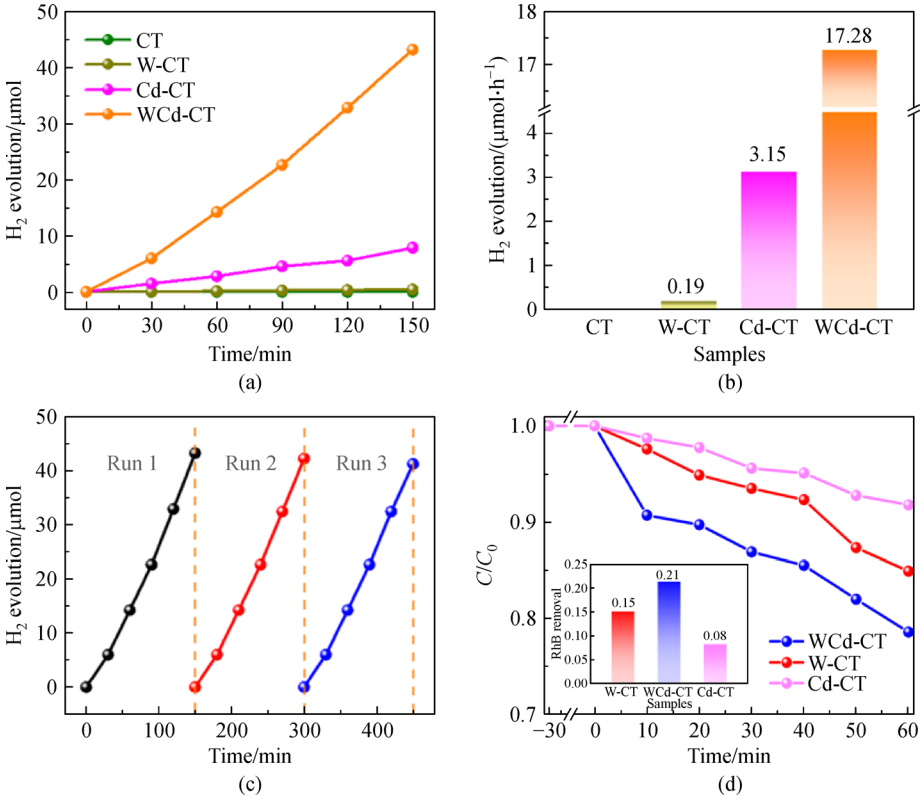

Fig. 6 Diagrams of photocatalytic performance of prepared samples.
(a) Time course hydrogen evolution of W-CT, Cd-CT, and WCd-CT; (b) comparison of hydrogen production rate of different samples; (c) cycling performance of WCd-CT in hydrogen production; (d) photocatalytic degradation performance under simulated solar light irradiation.

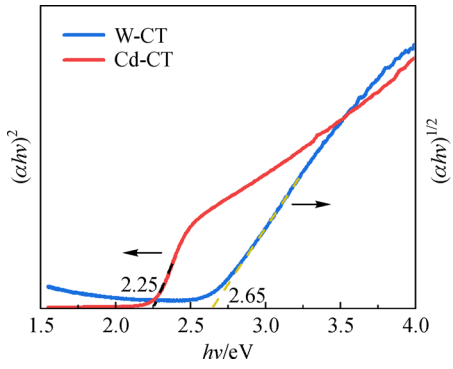

Fig. 7 Band gap width of CdS and WO_3.

WO_3, indicating the enhanced charge separation efficiency inside the prepared WCd-CT sample. Besides, a smaller semicircle in EIS Nyquist plot can be observed (Fig. 8(b)), indicating the faster migration of charge and lower charge-transfer resistance in WCd-CT. The enhancement of charge separation and migration significantly plays a great role in improving the photocatalytic performance of WCd-CT.

Based on the above experimental results and the related reports [18], a hydrogen production mechanism (Fig. 9) of WO_3/CdS composite photocatalyst was proposed. After the excitation of incident light, photogenerated electrons and holes were produced in WO_3 and CdS, respectively. The holes generated in WO_3 remain in the VB of WO_3, while electrons tend to transfer to the VB of CdS and recombine with the holes in CdS, so that the electrons and holes in CdS can be effectively separated. The holes stored in the VB of WO_3 would eventually be captured by the hole traps added in the solution, while the electrons in the CB of CdS would migrate to the surface and participate in water reduction. In addition, the improvement of hydrogen production activity is mainly attributed to the effective separation of photogenerated electron-hole pairs. At the same time, the composite photocatalyst retains a strong redox ability.

4 Conclusions

In summary, WO_3-CdS composite material was successfully loaded on the surface of carbon cloth using the hydrothermal methods. Profits from the construction of the Z-scheme system and the separation of photogenerated electron-hole pairs in the composite material had been significantly improved. Therefore, compared with pure W-CT and Cd-CT, the composite WCd-CT exhibited out-

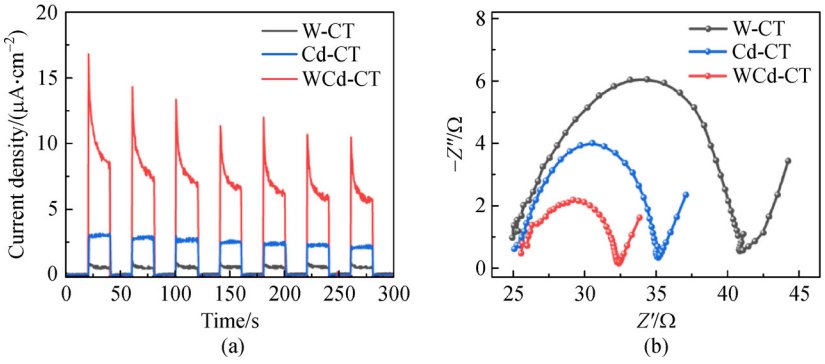

Fig. 8 Electrochemical analysis of prepared samples.
(a) Transient photocurrent of W-CT, Cd-CT, and WCd-CT; (b) electrochemical impedance spectra (EIS) of W-CT, Cd-CT, and WCd-CT.

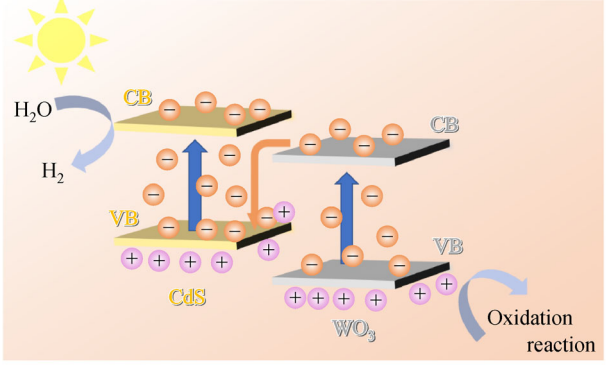

Fig. 9 Charge separation and transfer in CdS/WO_3 system under irradiation.

standing simulated sunlight driven photocatalytic activities. In the hydrogen production experiment, a superior H_2 generation rate of 17.28 μmol/h (about 4.5 times higher than that of Cd-CT) was reached when adding one piece of WCd-CT. At the same time, in the degradation test, the composite material also showed a better photodegradation activity. This study provides an idea for the immobilization of powder materials and creates conditions for better industrial applications of photocatalysts.

Acknowledgements This work was supported by the National Natural Science Foundation of China (Grant No. 21972040), the Program of Introducing Talents of Discipline to Universities (B20031), the Innovation Program of Shanghai Municipal Education Commission (2021-01-07-00-02-E00106), the Science and Technology Commission of Shanghai Municipality (20DZ2250400), and Fundamental Research Funds for the Central Universities.

Electronic Supplementary Material Supplementary material is available in the online version of this article at https://doi.org/10.1007/s11708-021-0768-6 and is accessible for authorized users.

References

1. Hayat A, Chen Z, Luo Z, et al. Π-deficient pyridine ring-incorporated carbon nitride polymers for photocatalytic H_2 evolution and CO_2 fixation. Research on Chemical Intermediates, 2021, 47(1): 15–27
2. Xu J, Mao M, Yu H. Functionalization of sheet structure Co-Mo-S with $Ni(OH)_2$ for efficient photocatalytic hydrogen evolution. Research on Chemical Intermediates, 2020, 46(3): 1823–1840
3. Turner J A. Sustainable hydrogen production. Science, 2004, 305 (5686): 972–974
4. Fujishima A, Honda K. Electrochemical photolysis of water at a semiconductor electrode. Nature, 1972, 238(5358): 37–38
5. Tang J, Gao B, Pan J, et al. CdS nanorods anchored with CoS_2 nanoparticles for enhanced photocatalytic hydrogen production. Applied Catalysis A: General, 2019, 588: 117281
6. Kumaravel V, Mathew S, Bartlett J, et al. Photocatalytic hydrogen production using metal doped TiO_2: a review of recent advances. Applied Catalysis B: Environmental, 2019, 244: 1021–1064
7. Sampaio M J, Oliveira J W L, Sombrio C I L, et al. Photocatalytic performance of Au/ZnO nanocatalysts for hydrogen production from ethanol. Applied Catalysis A: General, 2016, 518: 198–205
8. Zhu C, Liu C, Fu Y, et al. Construction of CDs/CdS photocatalysts for stable and efficient hydrogen production in water and seawater. Applied Catalysis B: Environmental, 2019, 242: 178–185
9. Shang L, Tong B, Yu H, et al. CdS nanoparticle-decorated Cd nanosheets for efficient visible light-driven photocatalytic hydrogen evolution. Advanced Energy Materials, 2016, 6(3): 1501241
10. Hao X, Wang Y, Zhou J, et al. Zinc vacancy-promoted photocatalytic activity and photostability of ZnS for efficient visible-light-driven hydrogen evolution. Applied Catalysis B: Environmental, 2018, 221: 302–311
11. Zhao J, Zhang Z, Chen X, et al. Microwave-induced assembly of $CuS@MoS_2$ core-shell nanotubes and study on their photocatalytic Fenton-like reactions. Acta Chimica Sinica, 2020, 78(9): 961–967
12. Prasad C, Tang H, Liu Q, et al. A latest overview on photocatalytic application of g-C_3N_4 based nanostructured materials for hydrogen production. International Journal of Hydrogen Energy, 2020, 45(1): 337–379
13. Kim D, Yong K. Boron doping induced charge transfer switching of a C_3N_4/ZnO photocatalyst from Z-scheme to type II to enhance photocatalytic hydrogen production. Applied Catalysis B: Environmental, 2021, 282: 119538
14. Yuan Y J, Chen D, Yu Z T, et al. Cadmium sulfide-based nanomaterials for photocatalytic hydrogen production. Journal of Materials Chemistry A, 2018, 6(25): 11606–11630
15. Wei R, Huang Z, Gu G, et al. Dual-cocatalysts decorated rimous CdS spheres advancing highly-efficient visible-light photocatalytic hydrogen production. Applied Catalysis B: Environmental, 2018, 231: 101–107
16. Wang D, Zeng H, Xiong X, et al. Highly efficient charge transfer in CdS-covalent organic framework nanocomposites for stable photocatalytic hydrogen evolution under visible light. Science Bulletin, 2020, 65(2): 113–122
17. Villa K, Murcia-López S, Andreu T, et al. Mesoporous WO_3 photocatalyst for the partial oxidation of methane to methanol using electron scavengers. Applied Catalysis B: Environmental, 2015, 163: 150–155
18. Jin J, Yu J, Guo D, et al. A hierarchical Z-scheme CdS-WO_3 photocatalyst with enhanced CO_2 reduction activity. Small, 2015, 11 (39): 5262–5271
19. Maeda K. Z-scheme water splitting using two different semiconductor photocatalysts. ACS Catalysis, 2013, 3(7): 1486–1503
20. Xu Q, Zhang L, Yu J, et al. Direct Z-scheme photocatalysts: principles, synthesis, and applications. Materials Today, 2018, 21 (10): 1042–1063
21. Niu X, Bai X, Zhou Z, et al. Rational design and characterization of direct Z-scheme photocatalyst for overall water splitting from excited state dynamics simulations. ACS Catalysis, 2020, 10(3): 1976–1983
22. Liu Q, Shen J, Yang X, et al. 3D reduced graphene oxide aerogel-mediated Z-scheme photocatalytic system for highly efficient solar-driven water oxidation and removal of antibiotics. Applied Catalysis B: Environmental, 2018, 232: 562–573
23. Zhou F, Fan J, Xu Q, et al. $BiVO_4$ nanowires decorated with CdS nanoparticles as Z-scheme photocatalyst with enhanced H_2 generation. Applied Catalysis B: Environmental, 2017, 201: 77–83
24. Wang S, Zhu B, Liu M, et al. Direct Z-scheme ZnO/CdS hierarchical photocatalyst for enhanced photocatalytic H_2-production activity. Applied Catalysis B: Environmental, 2019, 243: 19–26
25. Qiu B, Zhu Q, Du M, et al. Efficient solar light harvesting CdS/Co_9S_8 hollow cubes for Z-scheme photocatalytic water splitting. Angewandte Chemie International Edition, 2017, 56(10): 2684–2688
26. Cui H, Li B, Li Z, et al. Z-scheme based $CdS/CdWO_4$ heterojunction visible light photocatalyst for dye degradation and hydrogen evolution. Applied Surface Science, 2018, 455: 831–840
27. Balta Z, Bilgin Simsek E, Berek D. Solvothermal synthesis of WO_3/TiO_2/carbon fiber composite photocatalysts for enhanced performance under sunlight illumination. Photochemistry and

Photobiology, 2019, 95(6): 1331–1338

28. Li F, Chen L, Knowles G P, et al. Hierarchical mesoporous SnO_2 nanosheets on carbon cloth: a robust and flexible electrocatalyst for CO_2 reduction with high efficiency and selectivity. Angewandte Chemie International Edition, 2017, 56(2): 505–509
29. Vaiano V, Iervolino G. Facile method to immobilize ZnO particles on glass spheres for the photocatalytic treatment of tannery wastewater. Journal of Colloid and Interface Science, 2018, 518: 192–199
30. Huang Y, Guo Z, Liu H, et al. Heterojunction architecture of N-doped WO_3 nanobundles with Ce_2S_3 nanodots hybridized on a carbon textile enables a highly efficient flexible photocatalyst. Advanced Functional Materials, 2019, 29(45): 1903490
31. Wang J, Khoo E, Lee P S, et al. Synthesis, assembly, and electrochromic properties of uniform crystalline WO_3 nanorods. Journal of Physical Chemistry C, 2008, 112(37): 14306–14312
32. Kim C H, Kim B H, Yang K S. TiO_2 nanoparticles loaded on graphene/carbon composite nanofibers by electrospinning for increased photocatalysis. Carbon, 2012, 50(7): 2472–2481
33. Shi J, Cui H, Chen J, et al. TiO_2/activated carbon fibers photocatalyst: Effects of coating procedures on the microstructure, adhesion property, and photocatalytic ability. Journal of Colloid and Interface Science, 2012, 388(1): 201–208
34. Peng Q, Li Y, He X, et al. Interfacial enhancement of carbon fiber composites by poly(amido amine) functionalization. Composites Science and Technology, 2013, 74: 37–42
35. Gu L, Wang J, Cheng H, et al. One-step preparation of graphene-supported anatase TiO_2 with exposed {001} facets and mechanism of enhanced photocatalytic properties. ACS Applied Materials & Interfaces, 2013, 5(8): 3085–3093
36. Hu T, Li P, Zhang J, et al. Highly efficient direct Z-scheme WO_3/CdS-diethylenetriamine photocatalyst and its enhanced photocatalytic H_2 evolution under visible light irradiation. Applied Surface Science, 2018, 442: 20–29
37. Zhang L J, Li S, Liu B K, et al. Highly efficient CdS/WO_3 photocatalysts: Z-scheme photocatalytic mechanism for their enhanced photocatalytic H_2 evolution under visible light. ACS Catalysis, 2014, 4(10): 3724–3729